Published in final edited form as:
J Am Chem Soc. 2009 July 15; 131(27): 9562–9570. doi:10.1021/ja902291v.

Detection of Bacterial Spores with Lanthanide-Macrocycle Binary Complexes

Morgan L. Cable[§,†], **James P. Kirby**[†], **Dana J. Levine**[§,†], **Micah J. Manary**[§,†], **Harry B. Gray**[§], and **Adrian Ponce**[§,†]

Morgan L. Cable: ; James P. Kirby: james.p.kirby@jpl.nasa.gov; Dana J. Levine: ; Micah J. Manary: ; Harry B. Gray: hbgray@caltech.edu; Adrian Ponce: ponce@caltech.edu

[§]Beckman Institute, California Institute of Technology, Pasadena, California 91125

[†]Planetary Science Section, Jet Propulsion Laboratory, 4800 Oak Grove Drive, Pasadena, California 91109

Abstract

The detection of bacterial spores *via* dipicolinate-triggered lanthanide luminescence has been improved in terms of detection limit, stability, and susceptibility to interferents by use of lanthanide-macrocycle binary complexes. Specifically, we compared the effectiveness of Sm, Eu, Tb and Dy complexes with the macrocycle *1,4,7,10*-tetraazacyclododecane-*1,7*-diacetate (DO2A) to the corresponding lanthanide aquo ions. The $Ln(DO2A)^+$ binary complexes bind dipicolinic acid (DPA), a major constituent of bacterial spores, with greater affinity and demonstrate significant improvement in bacterial spore detection. Of the four luminescent lanthanides studied, the terbium complex exhibits the greatest dipicolinate binding affinity (100-fold greater than Tb^{3+} alone, and 10-fold greater than other $Ln(DO2A)^+$ complexes) and highest quantum yield. Moreover, the inclusion of DO2A extends the pH range over which Tb-DPA coordination is stable, reduces the interference of calcium ions nearly 5-fold, and mitigates phosphate interference 1000-fold compared to free terbium alone. In addition, detection of *Bacillus atrophaeus* bacterial spores was improved by the use of $Tb(DO2A)^+$, yielding a 3-fold increase in the signal-to-noise ratio over Tb^{3+}. Out of the eight cases investigated, the $Tb(DO2A)^+$ binary complex is best for the detection of bacterial spores.

Introduction

Bacterial spores (i.e., endospores) are dormant microbial forms that exhibit remarkable resistance to chemical and physical environmental stresses.[1-3] Because they are so resilient to most sterilization procedures, bacterial spores are used in several industries as biological indicators.[4,5] As these organisms are tough enough to survive even the extreme pressures, temperatures and radiation of space,[6] they are also the focus of research concerning panspermia and life in extreme environments.[7-9] In addition, detection of endospores became a national priority after the anthrax attacks of 2001, as *Bacillus anthracis* spore powders are the vectors of the anthrax bioweapon.[10-13] Rapid detection of DPA, a unique chemical marker and major constituent of bacterial spores,[14] is accomplished using DPA-sensitized lanthanide

Supporting Information Available: Crystallographic data (CIF) of the $Ln(DO2A)(DPA)^-$ complexes, where Ln = Sm, Eu, Tb or Dy; derivation of model for Ln(DPA) binding affinity; thermal ellipsoid plots of $Dy(DO2A)(DPA)^-$ ternary complex and Sm coordination geometry; normalized excitation and absorption spectra of $Ln(DO2A)(DPA)^-$ complexes; calculation of quantum yields and molar extinction coefficients for $Ln(DO2A)(DPA)^-$ complexes; K_a' values of $Tb(DO2A)(DPA)^-$ complex over time; emission spectra of various terbium, europium and samarium complexes; emission intensity variation in $Tb(DO2A)(DPA)^+$ due to interference from common cations and anions; ion competition experiments with phosphate, sulfate, potassium and carbonate; enthalpic and entropic components for $Tb(DO2A)(DPA)^-$ and $Eu(DO2A)(DPA)^-$; time courses of DPA binding to $Tb(DO2A)^+$ at various pH values; and calculation of signal-to-noise ratio for the bacterial spore detection study. This material is available free of charge via the Internet at http://pubs.acs.org.

luminescence under UV excitation. Enhancement of Tb^{3+} emission through an absorbance-energy transfer-emission (AETE) effect upon DPA coordination yields an increase in intensity by more than three orders of magnitude.[15-20] On average, DPA constitutes 10% of a bacterial spore's dry weight (10^8 molecules of DPA per spore); luminescence intensity of the Tb(DPA)$_3$·6H_2O complex can therefore be correlated to approximate spore concentration. This technique can be easily miniaturized and automated for rapid detection of a spore event[21] or possibly traces of life in extreme environments.

Although the method is rapid and straightforward, we aim to improve the Tb-DPA assay for detection of bacterial spores and expand our understanding of the chemistry underpinning this sensor system. The potential for false positives or false negatives through complexation of anionic interferents to the trivalent terbium cation is a serious concern when the method is applied to environmental samples. Previous studies indicate that phosphate in particular can inhibit DPA binding or decrease luminescence intensity.[22,23] Further, coordinated water molecules can quench Tb^{3+} luminescence by nearly an order of magnitude, due to radiationless deactivation from vibronic coupling of the OH oscillators with the excited lanthanide.[24] To eliminate water from the Tb^{3+}-coordination sphere and reduce the potential for interfering ion effects, we have introduced a macrocyclic ligand – DO2A (*1,4,7,10*-tetraazacyclododecane-*1,7*-diacetate) – to form a first-phase DPA receptor site. DO2A meets our initial conditions for a receptor site ligand, in that it binds strongly to Tb^{3+} (log K_{GdDO2A} = 19.42[25]) without impeding DPA binding. Our previous work using a binding affinity by competition (BAC) assay[26] demonstrates a two-order of magnitude increase in the DPA binding affinity with the $Tb(DO2A)^+$ binary complex over the Tb^{3+} aquo species.[27]

To design a receptor for a given analyte, we consider the following criteria: the receptor site must exhibit an obvious, measurable response upon analyte binding, meaning there must be a clear and distinguishable difference between the two states of analyte bound or unbound; the binding affinity should be high, on the order of $K \sim 10^9$ or greater;[28] binding kinetics should be proportional to the rate of analyte release and consistent with timescales for field work *in situ*; the receptor site should be resistant to local changes in the environment, such as pH and temperature variations; and binding to the receptor site should be highly selective, even in complex matrices containing common environmental interferents. The $Tb(DO2A)^+$ binary complex has met our initial conditions in improving lanthanide-based detection of dipicolinate; we now gear our analysis around these more stringent criteria in order to qualify this complex as an effective DPA receptor site.

Experimental Section

Materials

The following chemicals were purchased and used as received: ammonium chloride (J.T. Baker), calcium chloride trihydrate (Aldrich), CAPS (N-cyclohexyl-*3*-aminopropanesulfonic acid) buffer (Alfa Aesar), cesium chloride (MP Biomedicals), CHES (N-cyclohexyl-*2*-aminoethanesulfonic acid) buffer (Alfa Aesar), DPA (dipicolinic acid, pyridine-*2,6*,-dicarboxylic acid) (Aldrich), dysprosium(III) chloride hydrate (Alfa Aesar), europium(III) chloride hexahydrate (Aldrich), lithium chloride (Aldrich), magnesium chloride hexahydrate (Mallinckrodt), MES monohydrate (*2*-(N-morpholino)ethanesulfonic acid monohydrate) buffer (Alfa Aesar), MOPS (*3*-(N-morpholino)-propanesulfonic acid) buffer (Alfa Aesar), potassium chloride (Mallinckrodt), samarium(III) chloride (Alfa Aesar), sodium acetate trihydrate (Mallinckrodt), sodium bromide (J.T. Baker), sodium carbonate (Mallinckrodt), sodium chloride (EM Science), sodium citrate dihydrate (Mallinckrodt), sodium fluoride (Aldrich), sodium hydroxide (NaOH 50% in water) (Mallinckrodt), sodium iodide hydrate (Alfa Aesar), sodium nitrate (Mallinckrodt), sodium phosphate tribasic dodecahydrate (BDH), anhydrous sodium sulfate (Mallinckrodt), TAPS (N-tris(hydroxymethyl)methyl-*3*-

aminopropanesulfonic acid) buffer (TCI America), terbium(III) chloride hexahydrate (Alfa Aesar), tetrabutylammonium hydroxide (TBAOH 10% in 2-propanol) (TCI America) and L-tryptophan (Alfa Aesar). All lanthanide salts were 99.9% pure or greater, all other salts were 99% pure or greater, and all buffers were at least 98% pure. Water was deionized to a resistance of 18.2 MΩ-cm using a Siemens Purelab® Ultra laboratory water purification system. The *1,4,7,10*-tetraazacyclododecane-*1,7*-diacetate (DO2A) ligand was prepared by hydrolysis of *1,4,7,10*-tetraazacyclododecane-*1,7*-di(*t*-butyl acetate) (Macrocyclics), as described previously[27] resulting in a white solid in 99.8% yield. DO2A·2.80HCl·0.85H_2O. Anal. Calcd (found) for $C_{12}H_{24}N_4O_4$·2.80HCl·0.85H_2O (fw = 405.57): C, 35.54 (35.54); H, 7.08 (6.72); N, 13.81 (13.25); Cl, 24.43 (25.10). *Bacillus atrophaeus* bacterial spores were purchased from Raven Biological Laboratories and stored at 4°C until use.

Synthesis of Lanthanide Complexes—The procedure to generate the Ln(DO2A)$(DPA)^-$ ternary complex (Ln = Sm, Eu, Tb, Dy) as a tetrabutylammonium (TBA) salt has been described previously for the Tb and Eu species,[26,27] and is similar for the analogous Sm and Dy complexes. Slow crystallization from acetone yielded clear colorless (Eu, Tb, Dy) or yellow (Sm) crystals suitable for X-ray diffraction. **TBA·Sm(DO2A)(DPA)**. 0.474 g, yield: 44.8%. Anal. Calcd (found) in duplicate for $NC_{16}H_{36}$·$SmC_{19}H_{25}N_5O_8$·3.29H_2O·0.21$C_{16}H_{36}NCl$ (fw = 960.8): C, 47.88 (47.80); H, 7.87 (7.40); N, 9.05 (9.32); Sm, 15.65 (15.65). ESI-MS (*m/z*): calcd (found) for $SmC_{19}H_{25}N_5O_8$ (M^-) 603.4 (603.1). **TBA·Eu(DO2A)(DPA)**. 0.269 g, yield: 38.9%. Anal. Calcd (found) in duplicate for $NC_{16}H_{36}$·$EuC_{19}H_{25}N_5O_8$·3.52H_2O·0.93$C_{16}H_{36}NCl$ (fw = 1168.8): C, 51.32 (51.33); H, 8.77 (8.00); N, 8.31 (8.49); Eu, 13.00 (12.95). ESI-MS (*m/z*): calcd (found) for $EuC_{19}H_{25}N_5O_8$ (M^-) 604.4 (604.1). **TBA·Tb(DO2A)(DPA)**. 0.301 g, yield: 42.3%. Anal. Calcd (found) in duplicate for $NC_{16}H_{36}$·$TbC_{19}H_{25}N_5O_8$·1.00C_3H_6O· 4.00H_2O (fw = 982.97): C, 46.43 (46.63); H, 7.69 (8.17); N, 8.55 (8.71); Tb, 16.17 (15.65). ESI-MS (*m/z*): calcd (found) for $TbC_{19}H_{25}N_5O_8$ (M^-) 610.4 (610.1). **TBA·Dy(DO2A)(DPA)**. 0.102 g, yield: 45.4%. Anal. Calcd (found) in duplicate for $NC_{16}H_{36}$·DyC_{19} $H_{25}N_5O_8$·9.24H_2O·1.45$C_{16}H_{36}NCl$ (fw = 1426.9): C, 49.04 (49.05); H, 9.31 (7.66); N, 7.32 (8.68); Dy, 11.39 (11.40). ESI-MS (*m/z*): calcd (found) for $Dy_1C_{19}H_{25}N_5O_8$ (M^-) 615.4 (615.1).

Methods

Unless otherwise specified, all samples were prepared in triplicate to a final volume of 4.00 mL in disposable acrylate cuvettes (Spectrocell®), 1 cm pathlength, and were allowed to equilibrate for at least 24 hours before analysis using a Fluorolog-3 Fluorescence Spectrometer (Horiba Jobin-Yvon) at 25°C. To prevent the second-order diffraction of the source radiation, a 350-nm cutoff filter was used in all measurements. All reported spectra were obtained as a ratio of corrected signal to corrected reference (S_c/R_c) to eliminate the effect of varying background radiation in the sample chamber; emission intensities are in units of counts per second per microampere (cps/μA).

X-ray Crystallography—The crystal structures of TBA·Tb(DO2A)(DPA) and TBA·Eu(DO2A)(DPA) were described in previous work.[26,27] Diffraction data for the Sm and Dy complexes (Table 1) were collected at 100 ± 2 K on a Bruker SMART 1000 CCD area detector diffractometer equipped with graphite monochromated MoKα radiation (λα = 0.71073 Å). The structures were solved by isomorphous methods for Dy(DO2A)$(DPA)^-$ and direct methods for Sm(DO2A)$(DPA)^-$ and refined by full-matrix least-squares calculations on F^2 (SHELXL-97, Sheldrick, 1997). Non-hydrogen atoms were refined anisotropically. The hydrogen atoms were introduced in calculated positions. CCDC reference numbers 643596 and 655647.

Binary Complex Binding Studies—Association constants for Ln^{3+} to DPA^{2-} (Ln = Sm, Eu, Tb and Dy) were determined via titration of Ln^{3+} against 10.0 nM DPA in 0.2 M sodium

acetate (pH 7.4). A linear fit similar to that of the one-step equilibrium model of Jones and Vullev[22] was applied as $[Ln^{3+}] > [DPA^{2-}]$, and the binding affinity of the binary complex (K_a) was calculated using the following linear relationship:

$$\log\left(\frac{R}{C_{Ln}}\right)=\log(1-R)+\log K_a$$
$$R=\frac{[LnDPA]_{eq}}{[LnDPA]_{eq}+[DPA]_{eq}} \quad [1]$$

where C_{Ln} is the total concentration of the lanthanide and R is the normalized integrated emission intensity (see Supporting Information for derivation). This was performed for all four lanthanides at 10, 25, 35 and 50°C.

BAC Assay—Samples were prepared using solvated Ln(DO2A)(DPA)$^-$ crystals and lanthanide chloride salts in 0.2 M sodium acetate (pH 7.4), such that the concentration of Ln(DO2A)(DPA)$^-$ was 1.0 μM and the concentration of free Ln^{3+} ranged from 1.0 nM to 1.0 mM. Association constants were calculated using the Curve Fitting Tool in Matlab® with a Binding Affinity by Competition (BAC) chemical equilibrium model derived previously.[26]

Quantum Yields—Five concentrations ranging from 5.0 to 15.0 μM were prepared for each lanthanide complex in 0.1 M Tris (pH 7.9). Absorbance measurements were made in quartz cuvettes (1 cm pathlength) using a Cary 50 Bio UV/Visible Spectrophotometer, and luminescence measurements, also in quartz, were performed using the Fluorolog-3 Fluorescence Spectrometer (λ_{ex} = 280 nm). All recorded absorbances were under 0.1 and all luminescence intensities were below 5×10^5 cps (counts per second), well within the linear range of both instruments. Quantum yield measurements were standardized to L-tryptophan in deionized water (18.2 MΩ-cm resistance) at the same excitation wavelength, pH 5 (Φ_{ref} = 0.13 ± 0.01).[29] Corrections were made for the difference in refractive index between buffered H_2O (0.1 M Tris) and pure H_2O.

pH Dependence—For each lanthanide, samples were prepared in triplicate from 4.00 mM stock solutions of $LnCl_3$, DPA and DO2A to contain 10.0 μM Ln(DO2A)(DPA)$^-$ in 0.1 M buffer. Five buffers were used: MES (pK_a = 6.1), MOPS (pK_a = 7.2), TAPS (pK_a = 8.4), CHES (pK_a = 9.3) and CAPS (pK_a = 10.4), with pH adjustment to within 0.1 of the pK_a value using 50% NaOH added dropwise. Emission spectra were obtained after an equilibration time of 24 hours.

Temperature Dependence—The series of Tb(DO2A)(DPA)$^-$ cuvettes used in the BAC assay were heated or cooled to a specified temperature (eq. time of ~24 hrs for each temperature point) in the range of 10-50°C using a refrigerator (Marvel Scientific), incubator (VWR), or AccuBlock™ Digital Dry Bath (Labnet International). The sample chamber of the Fluorolog-3, which has a cuvette-holder that can be temperature-controlled, was connected to a Neslab RTE 7 Digital Plus water heater/chiller (Thermo Scientific) to maintain the desired temperature of the cuvette during scans. The temperature of each cuvette was checked prior to and following each measurement, and these values were averaged over the set of cuvettes to produce the reported temperature.

Cation/Anion Competition—Cuvettes were prepared with 0.10 μM Tb(DO2A)(DPA)$^-$ or Tb(DPA)$^+$ and an excess (100, 10, 1.0 or 0.10 mM) of one of the following ions: magnesium, calcium, lithium, sodium, potassium, ammonium, cesium, acetate, nitrate, fluoride, chloride, bromide, iodide, carbonate, sulfate, phosphate and citrate. All cations were chloride salts, and all anions were sodium salts. Solution pH was adjusted to ~7 with NaOH or HCl added

dropwise. Cations or anions of particular interest (calcium, phosphate, sulfate, potassium and carbonate) were used in competition experiments against 0.1 μM Tb(DO2A)(DPA)$^-$ in 0.1 M MOPS (pH 7.5), where the concentration of the ion was varied from 1.0 nM to 0.1 M. For ion experiments where significant competition was observed, the data was fit using the Curve Fitting Tool in Matlab® with a chemical equilibrium model similar to that used for the BAC Assay. We consider calcium as our example to derive this model. We start with the equilibrium described in [2], which has the corresponding equilibrium expression written in [3].

$$\mathrm{Tb(DO2A)(DPA)^- + Ca^{2+} \overset{K_{cation}}{\rightleftharpoons} Tb(DO2A)^+ + CaDPA} \quad [2]$$

$$K_{cation} = \frac{[\mathrm{Tb(DO2A)^+}]_{eq}\,[\mathrm{CaDPA}]_{eq}}{[\mathrm{Tb(DO2A)(DPA)^-}]_{eq}\,[\mathrm{Ca^{2+}}]_{eq}} \quad [3]$$

Since $K_{Tb(DO2A)} \gg K_{Ca(DO2A)}$,[30] we assume negligible formation of Ca(DO2A) or $TbDPA^+$. As $Tb(DO2A)^+$ and CaDPA form in a ratio of 1:1 from the dissociation of one Tb (DO2A)(DPA)$^-$, we obtain equation [4].

$$[\mathrm{Tb(DO2A)^+}]_{eq} = [\mathrm{CaDPA}]_{eq} \quad [4]$$

The total concentration of Tb^{3+} is expressed in [5], and similarly the total concentration of Ca^{2+} is given in [6].

$$[\mathrm{Tb^{3+}}]_{Tot} = [\mathrm{Tb\,(DO2A)\,(DPA)^-}]_{eq} + [\mathrm{Tb(DO2A)^+}]_{eq} \quad [5]$$

$$[\mathrm{Ca^{2+}}]_{Tot} = [\mathrm{Ca^{2+}}]_{eq} + [\mathrm{CaDPA}]_{eq} \quad [6]$$

Rearranging, we have [7] and [8]:

$$[\mathrm{Tb(DO2A)^+}]_{eq} = [\mathrm{Tb^{3+}}]_{Tot} - [\mathrm{Tb\,(DO2A)\,(DPA)^-}]_{eq} \quad [7]$$

$$[\mathrm{Ca^{2+}}]_{eq} = [\mathrm{Ca^{2+}}]_{Tot} - [\mathrm{CaDPA}]_{eq} = [\mathrm{Ca^{2+}}]_{Tot} - [\mathrm{Tb(DO2A)^+}]_{eq} \quad [8]$$

Substituting [4], [7] and [8] into [3], we have expression [9].

$$K_{cation} = \frac{\left\{[\mathrm{Tb}]_{Tot} - [\mathrm{Tb\,(DO2A)\,(DPA)^-}]_{eq}\right\}^2}{[\mathrm{Tb\,(DO2A)\,(DPA)^-}]_{eq}\left([\mathrm{Ca^{2+}}]_{Tot} - [\mathrm{Tb}]_{Tot} + [\mathrm{Tb\,(DO2A)\,(DPA)^-}]_{eq}\right)} \quad [9]$$

After some rearranging, we have:

$$(1 - K_{cation})\left\{[Tb(DO2A)(DPA)^{-}]_{eq}\right\}^2 + \left(K_{cation}[Tb^{3+}]_{Tot} - K_{cation}[Ca^{2+}]_{Tot} - 2[Tb^{3+}]_{Tot}\right)[Tb(DO2A)(DPA)^{-}]_{eq} + \left\{[Tb^{3+}]_{Tot}\right\}^2 = 0 \quad [10]$$

Solving for $[Tb(DO2A)(DPA)^{-}]_{eq}$, we have equation [11].

$$[Tb(DO2A)(DPA)^{-}]_{eq} = \frac{-A + \sqrt{A^2 - 4B\left\{[Tb^{3+}]_{Tot}\right\}^2}}{2B}$$

where

$$A = (K_{cation} - 2)[Tb^{3+}]_{Tot} - K_{cation}[Ca^{2+}]_{Tot}$$
$$B = 1 - K_{cation} \quad [11]$$

In terms of intensity, we need an expression in the form of [12], as only the terbium-containing species will be observable via luminescence measurements.

$$I_{obs} = c_1 I_1 + c_2 I_2$$

where

$$I_1 = \text{intensity of } [Tb(DO2A)(DPA)^{-}]_{eq}$$
$$I_2 = \text{intensity of } [Tb(DO2A)^{+}]_{eq}$$
$$c_1 = \frac{[Tb(DO2A)(DPA)^{-}]_{eq}}{[Tb(DO2A)(DPA)^{-}]_{Tot}}$$
$$c_2 = \frac{[Tb(DO2A)^{+}]_{eq}}{[Tb(DO2A)(DPA)^{-}]_{Tot}} = 1 - c_1 \quad [12]$$

Substituting in eq [11], we finally end with eq [13].

$$I_{obs} = \left(\frac{[Tb(DO2A)(DPA)^{-}]_{eq}}{[Tb(DO2A)(DPA)^{-}]_{Tot}}\right) I_1 + \left(1 - \frac{[Tb(DO2A)(DPA)^{-}]_{eq}}{[Tb(DO2A)(DPA)^{-}]_{Tot}}\right) I_2$$

where

$$[Tb(DO2A)(DPA)^{-}]_{eq} = \frac{-\left\{\left(10^{-7} - [Ca^{2+}]_{Tot}\right)K_{cation} - 2\left(10^{-7}\right)\right\} + \sqrt{\left\{\left(10^{-7} - [Ca^{2+}]_{Tot}\right)K_{cation} - 2\left(10^{-7}\right)\right\}^2 - 4(1 - K_{cation})\left\{[Tb^{3+}]_{Tot}\right\}^2}}{2(1 - K_{cation})} \quad [13]$$

This equation was used in the Matlab® Curve-Fit Toolbox to fit the calcium competition experiment data and calculate the competition constants.

Bacterial Spore Study—Approximately 100 μL of a *Bacillus atrophaeus* bacterial spore stock suspension (approx. concentration 10^9 spores/mL) was diluted to 500 μL in a sterile microcentrifuge tube with filter-sterilized deionized water (18.2 MΩ-cm resistance). The spores were washed twice via centrifugation (16,100 rcf for 20 min), decanting the supernatant

and resuspending the pellet in 500 μL of filter-sterilized deionized water. The washed spores were diluted 1:50 using filter-sterilized deionized water. Bacterial spore concentration was determined using enumeration under phase-contrast microscopy to be 3.11×10^7 ($\pm 6.11 \times 10^6$) spores/mL. The solution was then diluted to 1.00×10^5 spores/mL, and samples were prepared in quintuplicate as follows: two 2.97 mL aliquots of the spore suspension were transferred to two microwave tubes and sealed using a crimper. Ten microwave tubes, along with two sets of controls containing filter-sterilized deionized water, were autoclaved at 134° C for 45 min to lyse the spores and effect DPA release. The solution from each tube was transferred to a cuvette, to which either 30 μL of 100 μM $TbCl_3$ or Tb(DO2A) was added to the lysed spore suspensions and the control solutions. The excitation and emission spectra were obtained following ~30 seconds of thorough mixing.

Results and Discussion

Structural Characterization

Mass spectrometry, elemental analysis and the crystal structures confirm formation of all four Ln(DO2A)(DPA)$^-$ ternary complexes. With the exception of Eu(DO2A)(DPA)$^-$, all of the ternary complexes crystallized in the monoclinic space group $P2_1/c$. The Eu complex crystallized in the triclinic space group P1. The crystal structures of all four ternary complexes are superimposable (Sm structure shown in Figure 1A, Dy structure shown in Figure S2, Supporting Information), with slight differences (< 0.1 Å) appearing to follow the trend of Ln^{3+} ionic radius (Figure 1B). The coordination geometry of the lanthanide in each structure can be described as a slightly distorted capped staggered square bipyramidal conformation, with a pseudo-C2 axis passing through the DO2A core and the lanthanide (see Figure S3, Supporting Information).

Photophysics

Absorbance, luminescence excitation (λ_{Sm} = 600 nm, λ_{Eu} = 615 nm, λ_{Tb} = 544 nm, λ_{Dy} = 574 nm) and emission (λ_{ex} = 278 nm) spectra were obtained for each ternary complex. The emission spectra all display unique band splittings that are dependent on the site symmetry of the lanthanide coordination sphere, including those of Sm^{3+} ([Xe] $4f^5$) and Dy^{3+} ([Xe] $4f^9$), which exhibit Kramers' degeneracy in low symmetry cases.[31] For all four lanthanides this splitting is present in all observable emission peaks, regardless of hypersensitivity (i.e., the $^5D_0 \rightarrow {}^7F_2$ transition of Eu^{3+}), degeneracy of the lanthanide ground state, or whether assigned as electric dipole or magnetic dipole transitions. For example, emission spectra of the mono Dy $(DPA)^+ \cdot 6H_2O$ complex, the homoleptic $Dy(DPA)_3^{3-}$ species, and ternary Dy(DO2A)(DPA)$^-$ all exhibit very different splittings (Figure 2), and these characteristic differences can be used to visually identify the major component in solution. Emission spectra for the other three lanthanides are included in the Supporting Information.

The luminescence quantum yields for Tb complexes are greater than those of the Dy, Eu, and Sm complexes (Table 2). This is most likely due to (1) the small energy gap and corresponding strong coupling between the DPA triplet state and the terbium $^5D_4$ excited state,[32,33] and (2) the absence of other terbium excited states lower in energy than the DPA triplet, which might quench emission via nonradiative decay.[34] For the case of Dy, the quantum yield is lower despite an even smaller energy gap[35] (Table 3), because the $^4I_{15/2}$ and $^4G_{11/2}$ excited states are also populated and each contributing to the loss of quantum yield via nonradiative decay.[36] The high efficiency and intensity of the Tb complex confirm our choice of this lanthanide in the $Ln(DO2A)^+$ binary complex as the optimal dipicolinate receptor site.

Lanthanide Selection

We applied a method similar to that used by Jones and Vullev to calculate the binding affinity of Ln^{3+} and DPA^{2-} (Ln = Sm, Eu, Tb and Dy) at 25°C. Our results (Table 4) for the terbium case are in agreement with the formation constant obtained by Jones and Vullev at a similar pH.[22] Following calculation of the Ln-DPA binding affinity, the BAC assay[26] was utilized to calculate the association constant of the given $Ln(DO2A)^+$ binary complex for DPA^{2-} (Figure 3). As seen in Figure 4, the addition of the DO2A ligand enhances the binding affinity of the Ln^{3+} ion for DPA^{2-} by at least an order of magnitude. Interestingly, the binding affinity of the $Tb(DO2A)^+$ binary complex is even more effective, and nearly an order of magnitude greater than the other three lanthanides. This high order of stability is maintained for extended periods of time, approaching one year or more (see Table S2, Supporting Information). The BAC Assay was repeated at various temperatures for the Tb^{3+} and Eu^{3+} complexes; results indicate a nonlinear temperature dependence on the stability of the $Tb(DO2A)(DPA)^-$ complex over the range from 10-50°C, though a slight trend is observed for the Eu complex (Table 5). This is consistent with previous temperature dependence studies of europium complexes.[37]

Though others have noted that complex formation involving macrocyclic ligands can occur on the order of several hours to even days,[38-41] we have found that DPA binding is rapid at neutral to high pH provided that the $Tb(DO2A)^+$ binary complex is already formed in solution, as would be the case for a receptor site (see Figure S16, Supporting Information).

A pH dependence study was conducted over a range from 6.1 to 10.4 to determine the extent of ternary complex stability. The number of DPA molecules bound per lanthanide was calculated using the luminescence transition with the most obvious change in band splitting (i.e., the 'ligand field sensitive' peak) for the three complexes, $Ln(DPA)^+$, $Ln(DPA)_3^{3-}$ and $Ln(DO2A)(DPA)^-$, and solving each pH dependence emission spectrum as a best fit of a linear combination of these three profiles. Transitions used in calculation: Tb ($^5D_4 \rightarrow {}^7F_4$, 570 – 600 nm), Eu ($^5D_0 \rightarrow {}^7F_4$, 675 – 710 nm), Dy ($^4F_{9/2} \rightarrow {}^6H_{13/2}$, 555 – 595 nm), Sm ($^4G_{5/2} \rightarrow {}^6H_{7/2}$, 580 – 625 nm). With the DO2A ligand bound, a ratio of one DPA molecule per lanthanide is maintained over the entire pH range, meaning all four lanthanide ternary complexes remained stable (Figure 5). In contrast, the $Ln(DPA)^+$ complexes began to form the tris $Ln(DPA)_3^{3-}$ species at high pH as evidenced by the Ln:DPA ratio approaching 1:3, indicating precipitation of some of the lanthanide as $Ln(OH)_3$. This result indicates that the addition of the DO2A ligand prevents precipitation of the trivalent lanthanide cation and confers additional stability to the complex.

Interferents and Detection of Bacterial Spores

A screen was performed to test the robustness of the $Tb(DO2A)^+$ receptor site in the presence of common environmental interferents. Addition of common cations and anions in excess (three to six orders of magnitude) to nanomolar $Tb(DO2A)(DPA)^-$ at near neutral pH resulted in minimal emission intensity change for most ions in comparison to the $Tb(DPA)^+$ complex (see Figures S10-S13, Supporting Information). For most potential ionic interferents, the inclusion of DO2A improved luminescence intensity to some degree ($\leq 10^2$-fold) when the ion concentration was up to six orders of magnitude greater than the Tb-DPA concentration. Carbonate interference was only observed at concentrations five orders of magnitude or greater than that of Tb-DPA; in this regime, DO2A improves DPA sensing efficiency tenfold. Citrate interferes significantly with Tb-DPA complexation; this is mitigated with the use of DO2A for concentrations up to five orders of magnitude greater than Tb-DPA. DO2A complexation successfully eliminates phosphate interference for concentrations up to five orders of magnitude greater than Tb and DPA (Figure 6).

Competition experiments were performed for selected ions (see Figure S14, Supporting Information); of those, only calcium demonstrated any significant competition with Tb $(DO2A)^{+}$ for DPA^{2-}, and only at $\sim 10^4$ excess (Figure 7). This was expected, as CaDPA is a stable neutral salt (log $K_{CaDPA} = 4.05$[42]), and the mode by which most bacterial spores store the high concentration of dipicolinic acid present in the spore cortex.[14] The data were fit to a two-state chemical equilibrium model similar to that used in the BAC assay, and competition constants were calculated for Ca^{2+} competing with the $Tb(DO2A)^{+}$ binary complex (log $K_{cation} = -4.36 \pm 0.23$) and the Tb^{3+} ion alone (log $K_{cation} = -3.68 \pm 0.17$) for DPA^{2-}. The addition of the DO2A ligand improves the stability of Tb-DPA binding by a factor of 4.7 compared to the ion alone, increasing the range over which this receptor site can be used in environmental conditions.

Phosphate has been shown to severely inhibit DPA^{2-} binding to Tb^{3+} in previous studies, completely quenching Tb luminescence via an unknown mechanism even when DPA is in excess.[22,23] This was supported in the competition experiment for phosphate with Tb $(DPA)^{+}$; however, application of DO2A successfully mitigated phosphate interference in the binding of DPA^{2-} to Tb^{3+} by more than three orders of magnitude compared to Tb^{3+} alone (Figure 8).

With the superior stability and performance of the $Tb(DO2A)^{+}$ binary complex over Tb^{3+} alone verified experimentally, we have applied this novel DPA receptor site to the detection of actual bacterial spores. *Bacillus atrophaeus* bacterial spores have been well characterized in the literature[43-45] and represent spores found in typical environmental samples in their relative size and DPA content.[8,47] The use of DO2A in the detection of real bacterial spores not only doubles the luminescence intensity, but also improves the signal-to-noise ratio threefold (Figure 9). It is important to note that this result was achieved for low concentrations of bacterial spores without any sample purification (filtration to remove cell debris, extraction, pH adjustment, etc.), minimizing sample preparation while maximizing endospore detection.

Concluding Remarks

The $Ln(DO2A)(DPA)^{-}$ series (Ln = Sm, Eu, Tb and Dy) has been fully characterized. Close coupling of the DPA triplet excited state to the terbium $^5D_4$ excited state is responsible for enhanced intramolecular energy transfer in the $Tb(DO2A)(DPA)^{-}$ complex compared to the other three luminescent lanthanides studied and supports the observed trend in quantum yield. The application of DO2A successfully mitigates both cationic and anionic interferents of Tb-DPA luminescence, even those as notorious as phosphate. DO2A also exhibits a substantial improvement in the signal-to-noise ratio in the detection of DPA from lysed *B. atrophaeus* spores. We therefore conclude that the $Tb(DO2A)^{+}$ binary complex is a rapid, robust DPA receptor for the detection of bacterial spores.

Supplementary Material

Refer to Web version on PubMed Central for supplementary material.

Acknowledgments

MLC thanks Larry Henling and Mike Day for crystallographic analysis, and Kyle Lancaster for assistance with mass spectrometry. The research described in this paper was carried out at the Jet Propulsion Laboratory, California Institute of Technology, under contract with the National Aeronautic and Space Administration and was sponsored by NASA's Astrobiology and Planetary Protection Programs (AP, JPK), the Department of Homeland Security's Chemical and Biological Research & Development Program (AP), the National Defense Science and Engineering Graduate Fellowship Program (MLC), the NASA Graduate Student Research Program (MLC), the AmGen Scholars Program (DJL), and the Caltech Summer Undergraduate Research Fellowship Program (DJL, MJM). Work at the Beckman Institute was supported by NIH, NSF and the Arnold and Mabel Beckman Foundation (HBG).

References

1. Bisset KA. Nature 1950;166:431–432. [PubMed: 14775699]
2. Driks A. Proc Nat Acad Sci U S A 2003;100:3007–3009.
3. Nicholson WL, Munakata N, Horneck G, Melosh HJ, Setlow P. Microbiol Mol Biol Rev 2000;64:548–572. [PubMed: 10974126]
4. Albert H, Davies DJG, Woodson LP, Soper CJ. J Appl Microbiol 1998;85:865–874. [PubMed: 9830122]
5. Yung PT, Ponce A. Appl Environ Microbiol 2008;74:7669–7674. [PubMed: 18836020]
6. Horneck G, Bucker H, Reitz G. Adv Space Res 1994;14:41–45. [PubMed: 11539977]
7. Yung PT, Shafaat HS, Connon SA, Ponce A. FEMS Microbiol Ecol 2007;59:300–306. [PubMed: 17313579]
8. Shafaat HS, Ponce A. Appl Environ Microbiol 2006;72:6808–6814. [PubMed: 17021233]
9. Nicholson WL. Orig Life Evol Biosph 2003;33:621–631. [PubMed: 14601931]
10. Jernigan JA, Stephens DS, Ashford DA, Omenaca C, Topiel MS, Galbraith M, Tapper M, Fisk TL, Zaki S, Popovic T, Meyer RF, Quinn CP, Harper SA, Fridkin SK, Sejvar JJ, Sephard CW, et al. Emerg Infect Dis 2001;7:933–944. [PubMed: 11747719]
11. Sanderson WT, Stoddard RR, Echt AS, Piacitelli CA, Kim D, Horan J, Davies MM, McCleery RE, Muller P, Schnorr TM, Ward EM, Hales TR. J Appl Microbiol 2004;96:1048–1056. [PubMed: 15078521]
12. Yung PT, Lester ED, Bearman G, Ponce A. Biotech Bioeng 2007;84:864–871.
13. Sharp RJ, Roberts AG. J Chem Technol Biotechnol 2006;81:1612–1625.
14. Murrell, WG. The Bacterial Spore. Academic Press; New York: 1969.
15. Horrocks WD Jr, Sudnick DR. Acc Chem Res 1981;14:384–392.
16. Horrocks WD Jr, Albin M. Prog Inorg Chem 1984;31:1–104.
17. Balzani V. Pure Appl Chem 1990;62:1099–1102.
18. Balzani V, Decola L, Prodi L, Scandola F. Pure and Appl Chem 1990;62:1457–1466.
19. Hindle AA, Hall EAH. Analyst 1999;124:1599–1604. [PubMed: 10746319]
20. Lehn JM. Angew Chem Int Ed Engl 1988;27:89–112.
21. Lester ED, Bearman G, Ponce A. IEEE Eng Med Biol Mag 2004;23:130–135. [PubMed: 15154269]
22. Jones G, Vullev VI. J Phys Chem A 2002;106:8213–8222.
23. Pellegrino PM, Fell NF, Rosen DL, Gillespie JB. Anal Chem 1998;70:1755–1760.
24. Kropp JL, Windsor MW. J Phys Chem 1967;71:477–482.
25. Kim WD, Hrncir DC, Kiefer GE, Sherry AD. Inorg Chem 1995;34:2225–2232.
26. Kirby JP, Cable ML, Levine DJ, Gray HB, Ponce A. Anal Chem 2008;80:5750–5754. [PubMed: 18578548]
27. Cable ML, Kirby JP, Sorasaenee K, Gray HB, Ponce A. J Am Chem Soc 2007;129:1474–1475. [PubMed: 17243674]
28. Nogrady, T.; Weaver, DF. Medicinal Chemistry: A Molecular and Biochemical Approach. Oxford University Press; 2005. p. 67-105.
29. Chen RF. Anal Lett 1967;1:35–42.
30. Chang CA, Chen YH, Chen HY, Shieh FK. J Chem Soc, Dalton Trans 1998:3243–3248.
31. Görller-Walrand, C.; Binnemans, K. Handbook on the Physics and Chemistry of Rare Earths. Gschneidner, JKA.; Eyring, L., editors. Vol. 23. Elsevier Science B. V.; New York: 1996. p. 122-283.
32. Arnaud N, Vaquer E, Georges J. Analyst 1998;123:261–265.
33. Latva M, Takalo H, Mukkala VM, Matachescu C, RodriguezUbis JC, Kankare J. J Lumin 1997;75:149–169.
34. Carnall WT, Fields PR, Rajnak K. J Chem Phys 1968;49:4447–4449.
35. Hemmila I, Laitala V. J Fluor 2005;15:529–542.
36. Carnall WT, Fields PR, Rajnak K. J Chem Phys 1968;49:4424–4442.

37. Yerly F, Dunand Frank A, Tóth É, Figueirinha A, Kovács Z, Sherry AD, Geraldes CFGC, Merbach André E. Eur J Inorg Chem 2000;2000:1001–1006.
38. Kumar K, Jin TZ, Wang XY, Desreux JF, Tweedle MF. Inorg Chem 1994;33:3823–3829.
39. Wang X, Jin T, Comblin V, Lopez-Mut A, Merciny E, Desreux JF. Inorg Chem 1992;31:1095–1099.
40. Brucher E, Laurenczy G, Makra ZS. Inorg Chim Acta 1987;139:141.
41. Huskens J. Inorg Chem 1997;36:1495–1503. [PubMed: 11669731]
42. Chung L, Rajan KS, Merdinge E, Grecz N. Biophys J 1971;11:469–482. [PubMed: 5569493]
43. Fritze D, Pukall R. Int J Syst Evol Microbiol 2001;51:35–37. [PubMed: 11211269]
44. Setlow P. J Appl Microbiol 2006;101:514–525. [PubMed: 16907802]
45. Kunst F, Ogasawara N, Moszer I, Albertini AM, Alloni G, Azevedo V, Bertero MG, Bessières P, Bolotin A, Borchert S, Borriss R, Boursier L, Brans A, Braun M, Brignell SC, Bron S, et al. Nature 1997;390:249–256. [PubMed: 9384377]
46. Fichtel J, Koster J, Rullkotter J, Sass H. FEMS Microbiol Ecol 2007;61:522–532. [PubMed: 17623026]
47. Sojka B, Ludwig H. Pharm Ind 1997;59:355–359.
48. Sharma PK, Van Doorn AR, Staring AGJ. J Lumin 1994;62:219–225.
49. Carnall WT, Fields PR, Rajnak K. J Chem Phys 1968;49:4450–4455.

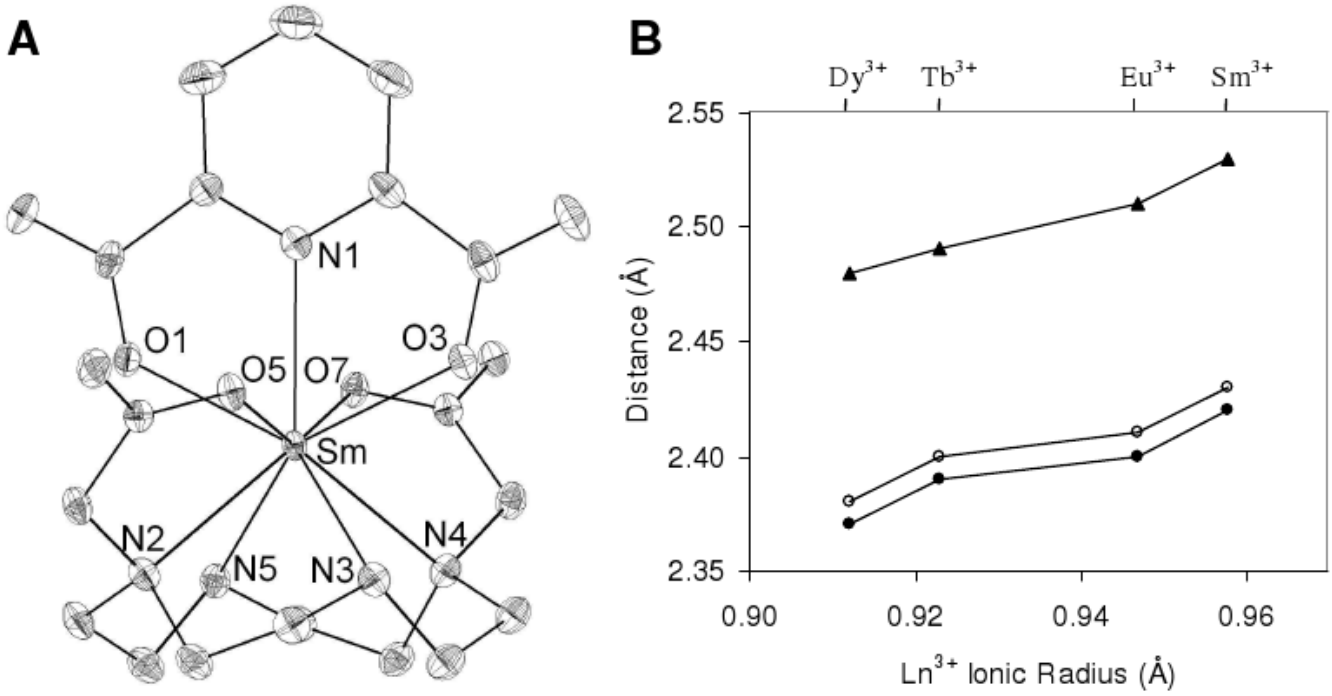

Figure 1.

(A) Thermal ellipsoid plot of the Sm(DO2A)(DPA)$^{-}$ ternary complex with 50% probability. Hydrogens omitted for clarity. (B) Plot of Ln^{3+}---DPA interatomic distances for the four ternary complex crystal structures against Ln^{3+} ionic radius. Ln—N1 distance (▲); Ln—O1 distance (●); Ln—O3 distance (○).

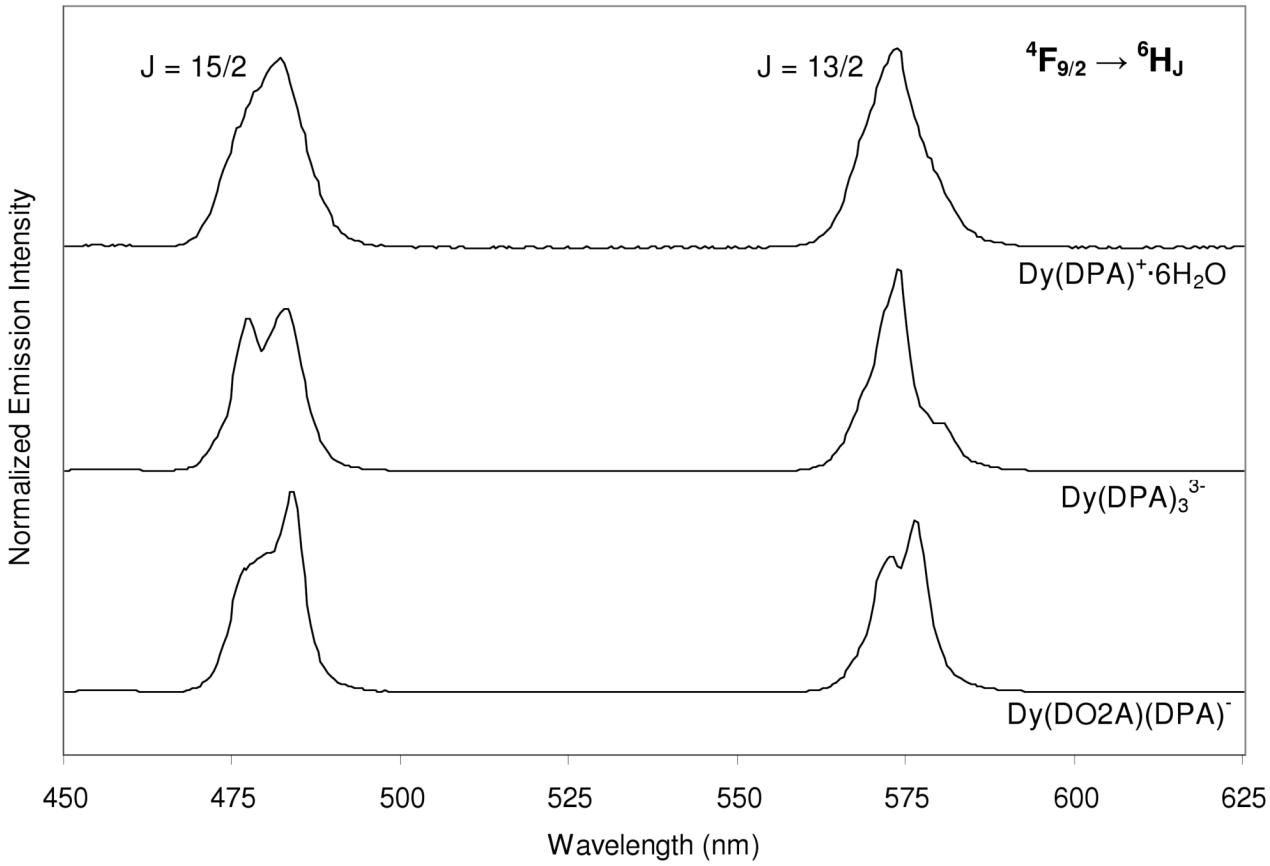

Figure 2.
Emission spectra of dysprosium complexes, 10.0 μM in 0.2 M sodium acetate, pH 7.4 (λ_{ex} = 278 nm).

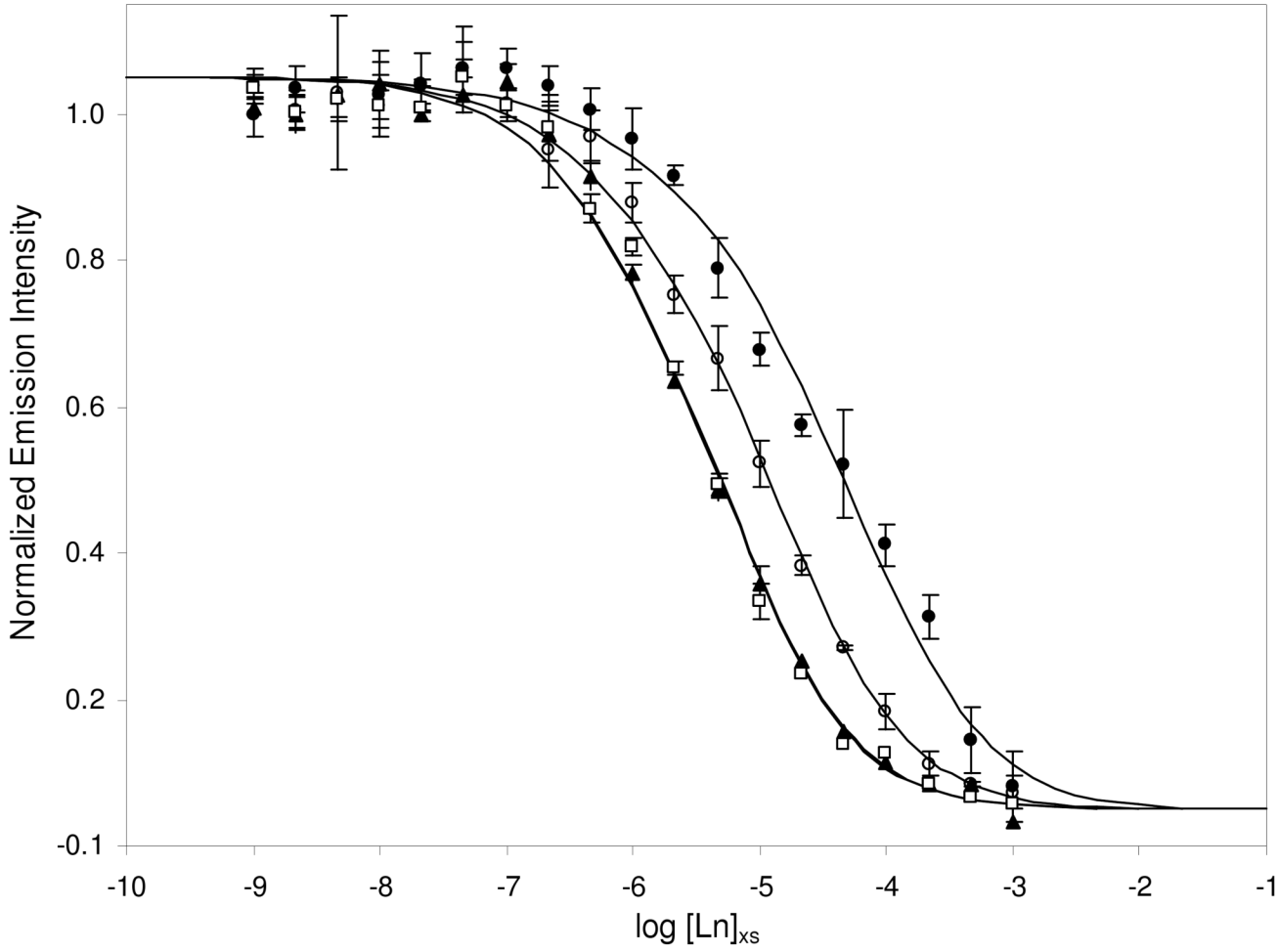

Figure 3.

BAC Assay applied to the four Ln(DO2A)(DPA)$^{-}$ ternary complexes (Ln = Sm □, Eu ▲, Tb ●, Dy ○) to determine the binding affinity of the Ln(DO2A)$^{+}$ binary complex for the DPA^{2-} analyte, 0.2 M sodium acetate, pH 7.5 (λ_{ex} = 278 nm).

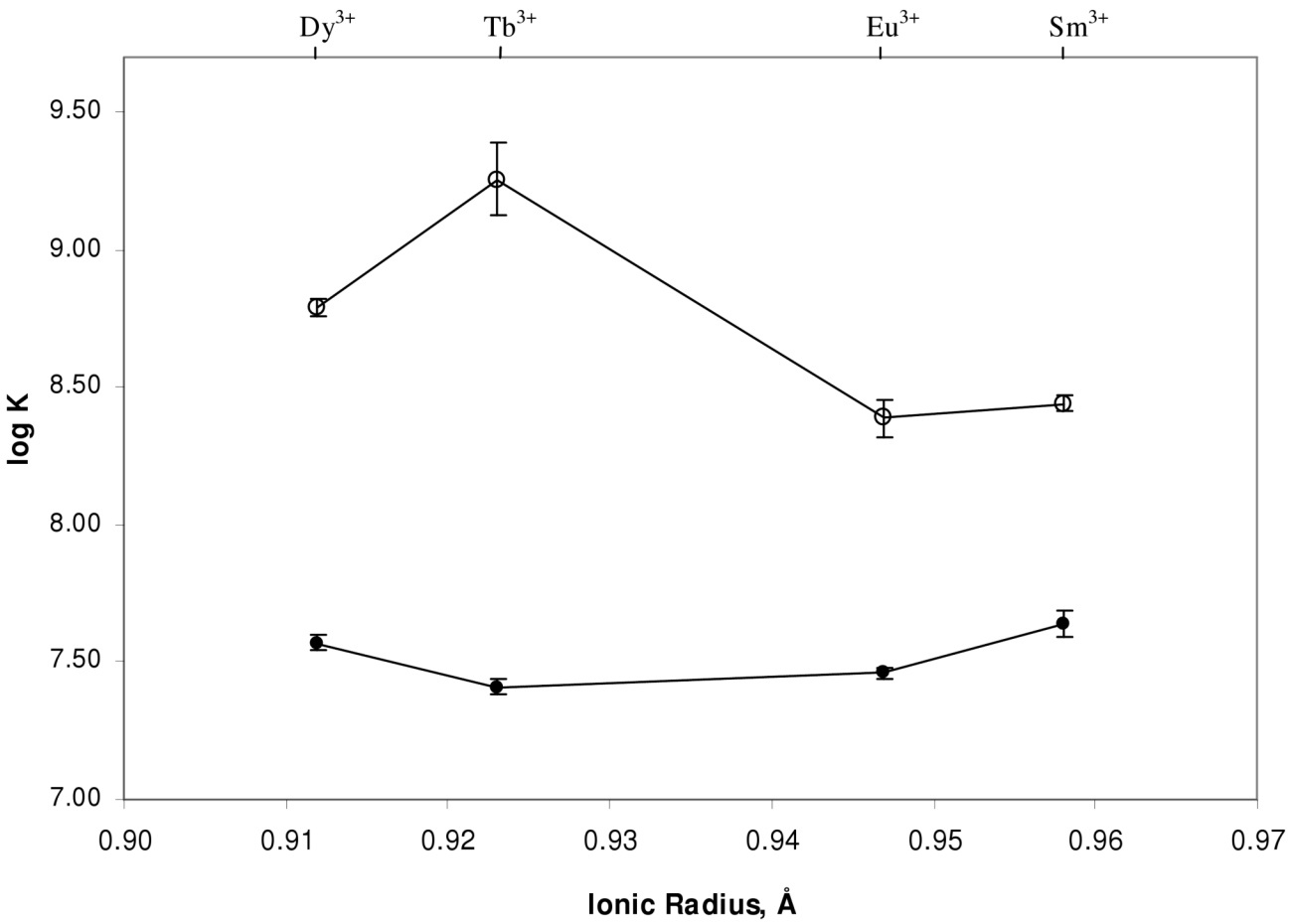

Figure 4.
Association constants of Ln^{3+} (●) and $Ln(DO2A)^{+}$ (○) to DPA^{2-} against lanthanide ionic radius, 0.2 M sodium acetate, pH 7.5, 25°C (λ_{ex} = 278 nm).

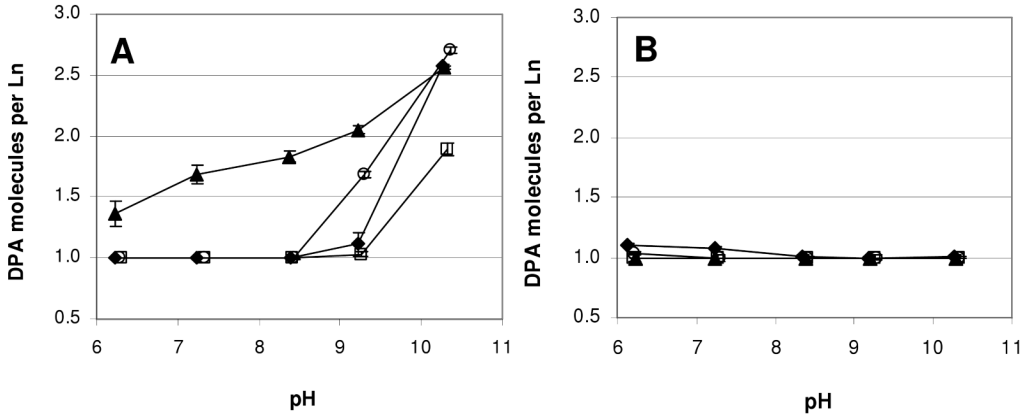

Figure 5.

Number of DPA molecules bound per Ln^{3+} as a function of pH for (A) $Ln(DPA)^{+}$ and (B) Ln (DO2A)$(DPA)^{-}$ complexes (Ln = Sm □, Eu ▲, Tb ◆, Dy ○), 10.0 μM in 0.1 M buffer (λ_{ex} = 278 nm).

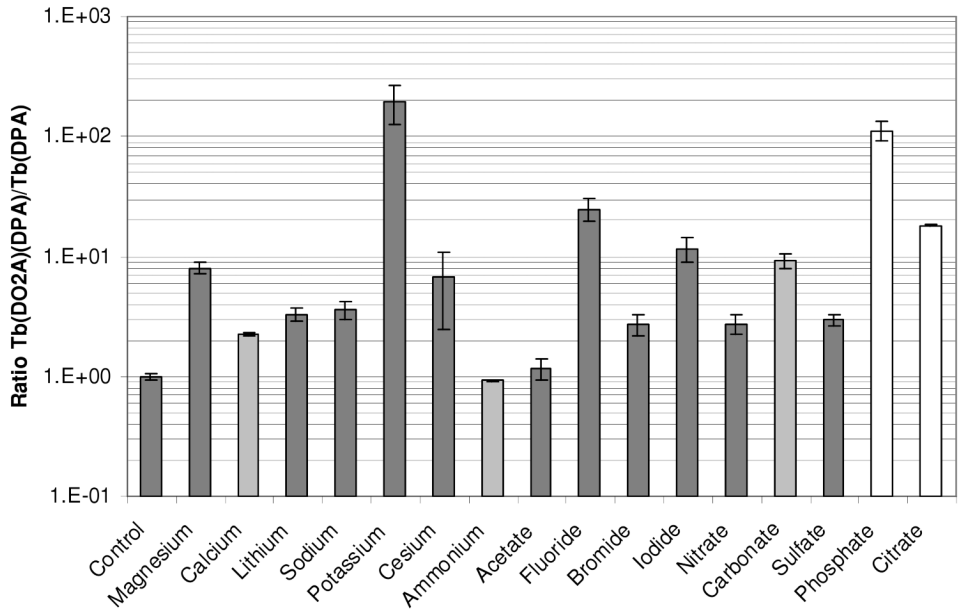

Figure 6.

Ratio of emission intensity (λ_{em} = 530 – 560 nm, λ_{ex} = 278 nm) of 0.1 μM Tb(DO2A)(DPA)$^{-}$ complex to 0.1 μM Tb(DPA)$^{+}$ complex in the presence of 100 mM (dark gray), 10 mM (light gray) or 1 mM (white) competing ion at pH 6.6.

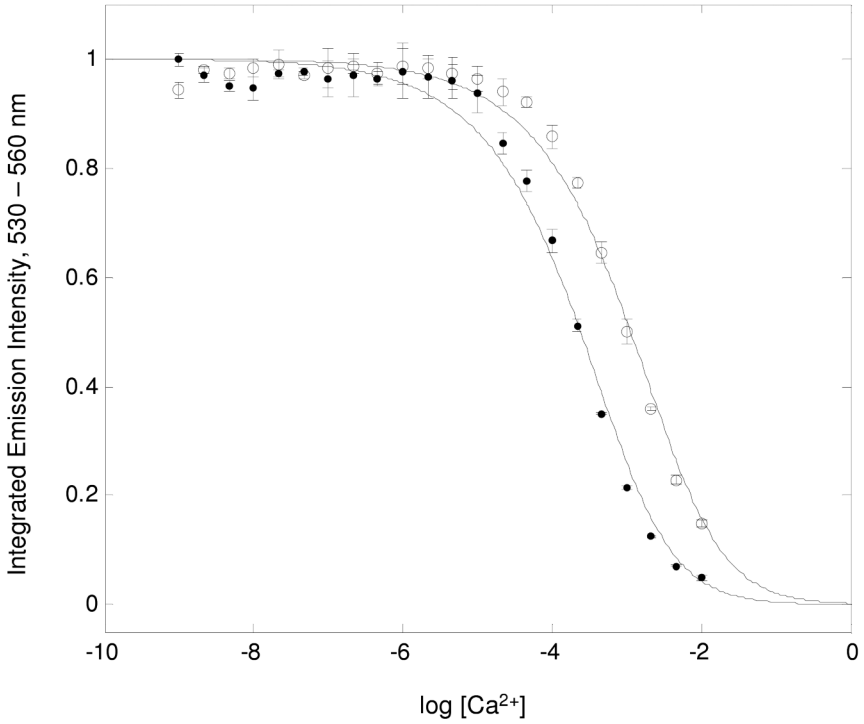

Figure 7.
Cation competition experiment of 0.1μM Tb(DO2A)(DPA)$^{-}$ (○) or Tb(DPA)$^{+}$ (●) titrated with Ca^{2+} over a concentration range from 1.0 nM to 0.1 M, pH 7.5 (0.1 M MOPS).

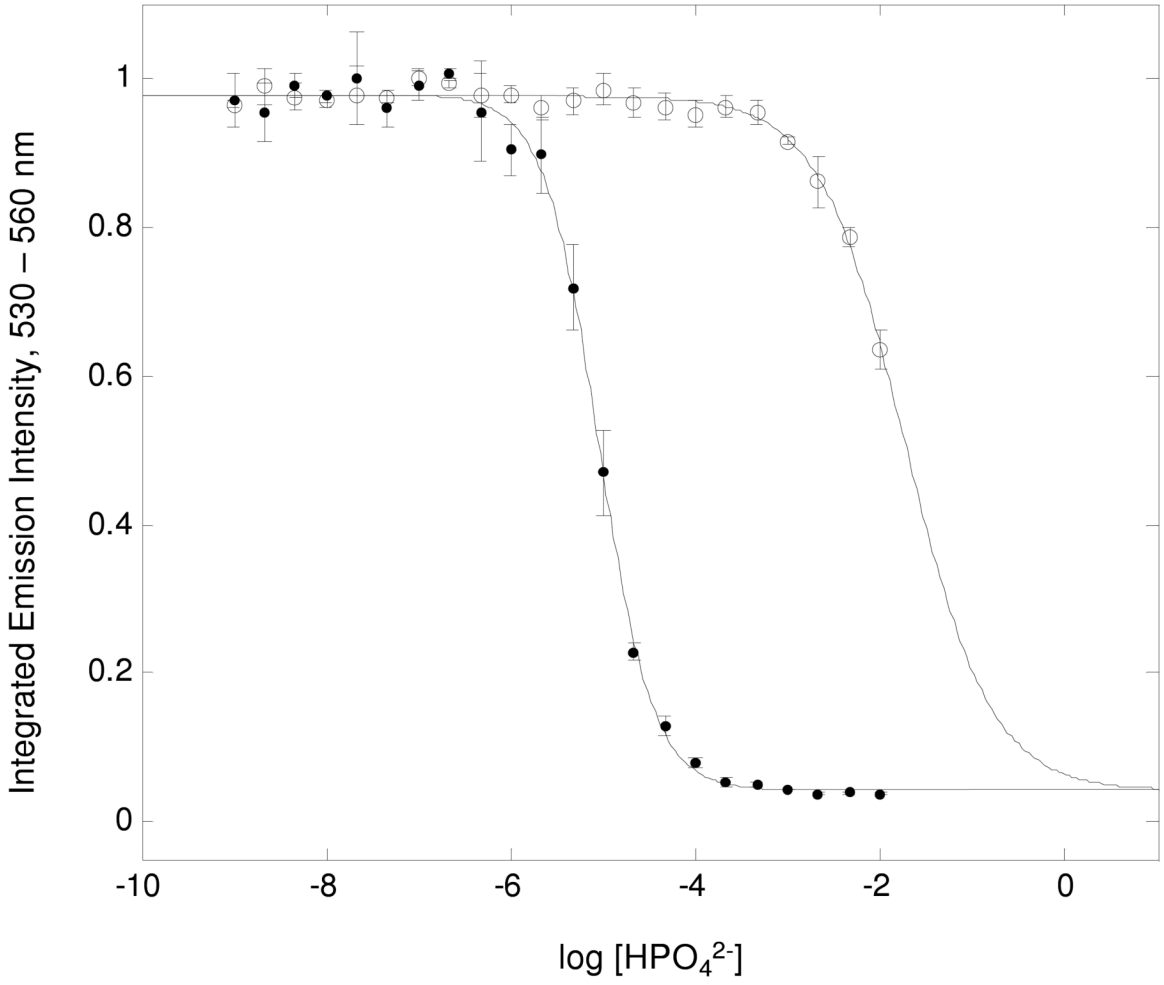

Figure 8.
Anion competition experiment of 0.1μM Tb(DO2A)(DPA)$^{-}$ (○) or Tb(DPA)$^{+}$ (●) titrated with phosphate over a concentration range from 1.0 nM to 0.1 M, pH 7.3 (0.1 M MOPS).

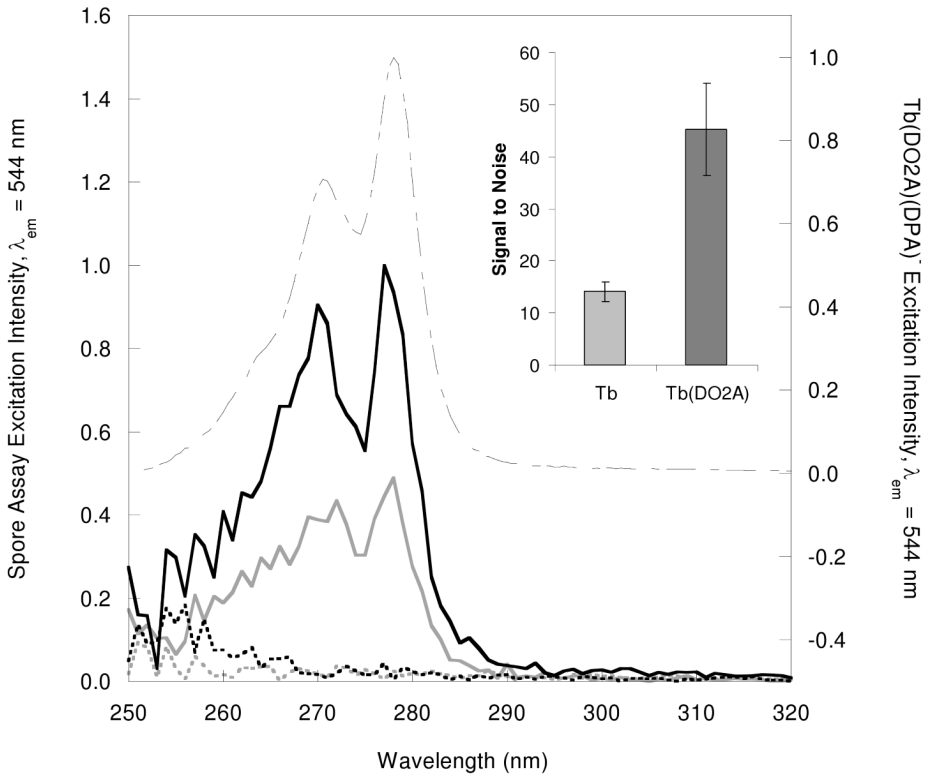

Figure 9.

Excitation spectra of unfiltered samples of autoclaved *Bacillus atrophaeus* spores containing 10 μM Tb^{3+} alone (gray solid) or the $Tb(DO2A)^{+}$ binary complex (black solid) in filter-sterilized nanopure H_2O. Dashed offset excitation spectrum of 10 μM Tb(DO2A)(DPA) in 0.2 M sodium acetate, pH 7.4, confirms excitation profile as DPA. Concentration of bacterial spores approx. 10^5 spores/mL. Controls of Tb^{3+} or $Tb(DO2A)^{+}$ are shown in dotted gray and black, respectively. Inset: Signal-to-noise ratio of emission intensity, 530 – 560 nm, for Tb^{3+} (light gray) and $Tb(DO2A)^{+}$ (dark gray), showing a three-fold improvement in S/N with the use of DO2A.

Table 1

Crystallographic data for the four TBA·Ln(DO2A)(DPA) structures.

Ln	**Tb**[§]	**Eu**[†]	**Dy**	**Sm**
Formula	$[C_{19}H_{25}N_5O_8Tb]^-$ $[C_{16}H_{36}N]^+\cdot$ $0.47(C_3H_8O)$ $0.53(C_3H_6O)$ $3(H_2O)$	$[C_{19}H_{25}N_5O_8Eu]^-$ $[C_{16}H_{36}N]^+\cdot$ $0.68(C_3H_8O)$ $0.32(C_3H_6O)$ $3(H_2O)$	$[C_{19}H_{25}N_5O_8Dy]^-$ $[C_{16}H_{36}N]^+\cdot$ $2(C_3H_8O)$ $3(H_2O)$	$[C_{19}H_{25}N_5O_8Sm]^-$ $[C_{16}H_{36}N]^+\cdot$ $0.27(C_2H_6O\cdot O)$ $0.73(C_3H_6O)$ $2(H_2O)$
M_w	964.94	957.23	966.51	939.36
Crystal system	Monoclinic	Triclinic	Monoclinic	Monoclinic
Space group	$P2_1/c$	P1	$P2_1/c$	$P2_1/c$
a (Å)	13.1047(5)	13.1473(4)	13.1742(4)	13.0658(4)
b (Å)	13.3397(5)	13.2269(4)	13.1860(4)	13.4504(4)
c (Å)	26.0901(9)	26.2248(8)	26.1130(8)	26.1778(7)
β (°)	90.0130(10)	90.0540(10)	90.3720(10)	90.3240(10)
V ($Å^3$), Z	4560.9(3)	4560.4(2)	4536.1(2)	4600.4(2)
λ (Å)	0.71073	0.71073	0.71073	0.71073
D_c (Mg/m^3)	1.405	1.394	1.415	1.356
μ, Mo-Kα (mm^{-1})	1.613	1.438	1.710	1.336
T (K)	100(2)	100(2)	100(2)	100(2)
R_1, wR_2[‡]	0.0384, 0.0639	0.0437, 0.0750	0.0408, 0.0721	0.0422, 0.0734

[§]Previous work.[27]

[†]Previous work.[26]

[‡]Structure was refined on F^2 using all reflections: $wR_2 = [\Sigma[w(F^2 - F_c^2)^2]/\Sigma w(F^2)^2]^{1/2}$, where $w^{-1} = [\Sigma(F^2) + (aP)^2 + bP]$ and $P = [\max(F^2,0) + 2F_c^2]/3$.

Table 2

Luminescence quantum yield data, 0.1 M Tris buffer, L-Trp standard.

Complex	Temp (°C)	pH	Φ_L
Sm(DO2A)(DPA)$^-$	25.4 ± 0.3	7.93 ± 0.02	0.001 ± 3E-05
Eu(DO2A)(DPA)$^-$	24.7 ± 0.1	7.92 ± 0.02	0.008 ± 3E-05
Tb(DO2A)(DPA)$^-$	24.8 ± 0.2	7.93 ± 0.01	0.110 ± 0.002
Dy(DO2A)(DPA)$^-$	25.6 ± 0.3	7.87 ± 0.02	0.006 ± 0.0001

Table 3

Ligand energy levels and lanthanide ion resonance levels involved in the absorbance-energy transfer-emission (AETE) mechanism of DPA-sensitized lanthanide luminescence.

Ligand Energy Level (cm^{-1})		Ln^{3+} Ion Resonance Level (cm^{-1})	
DPA Triplet	26,600[48]	Sm^{3+} $^4G_{5/2}$	17,900[36]
		Eu^{3+} $^5D_0$	17,264[49]
		Tb^{3+} $^5D_4$	20,500[34]
		Dy^{3+} $^4F_{9/2}$	21,100[36]

Table 4

Association constants of Ln^{3+} and $Ln(DO2A)^{+}$ with DPA^{2-}, calculated using a one-step equilibration model and the BAC Assay, respectively, pH 7.5.

Ln	log K_a	log K_a'
Sm	7.64 ± 0.05	8.44 ± 0.03
Eu	7.46 ± 0.02	8.39 ± 0.07[§]
Tb	7.41 ± 0.03	9.25 ± 0.13[†]
Dy	7.57 ± 0.03	8.79 ± 0.03

[§] Previous work.[26]

[†] Previous work.[27]

Table 5

Temperature dependence of association constants (log K_a') of $Ln(DO2A)^+$ and DPA^{2-} calculated using BAC Assay.

Temp (°C)	Tb	Eu
10.8	9.09 ± 0.04	8.49 ± 0.01
25.0	9.25 ± 0.13[§]	8.39 ± 0.07[†]
34.8	9.00 ± 0.08	8.25 ± 0.07
50.0	8.68 ± 0.05	7.93 ± 0.03

[§] Previous work.[27]

[†] Previous work.[26]